Examining sorption of perfluoroalkyl substances (PFAS) in biochars and other carbon-rich materials

Joel Fabregat-Palau, Miquel Vidal, Anna Rigol*

Department of Chemical Engineering and Analytical Chemistry, University of Barcelona, Martí i Franquès 1-11, 08028 Barcelona, Spain

ABSTRACT

The use of carbon-rich sorbents to remove and/or immobilize perfluoroalkyl substances (PFAS) in contaminated environmental scenarios is attracting increasing interest. The identification of key sorbent properties responsible for PFAS sorption and the development of models that can predict the distribution coefficients (K_d) for PFAS sorption in these materials are crucial in the screening of candidate materials for environmental remediation. In this study, sorption kinetics, sorption isotherms, and the effects of pH, calcium concentration and dissolved organic carbon (DOC) content on PFAS sorption were evaluated in four representative carbon-rich materials: two biochars with contrasting properties, a compost, and charcoal fines rejected by the metallurgical industry. Subsequently, the sorption of seven PFAS with numbers of fluorinated carbons ranging from 4 to 11 was evaluated in a total of ten carbon-rich materials, including activated carbons, so as to build up a K_d prediction model. The sorption of PFAS increased with greater fluorinated chain length, suggesting that hydrophobic interactions play a major role in sorption and electrostatic interactions a minor one. These results were confirmed by a principal component analysis, which revealed that the C_{ORG}/O molar ratio and the specific surface area of the material were the two main sorbent properties affecting PFAS sorption. Furthermore, the DOC content in solution had a negative effect on PFAS sorption. Using this information, a simple K_d prediction model applicable to a wide range of materials and PFAS was developed, using only a few easily-derived sorbent and PFAS physicochemical properties, and was externally validated with data gathered from the literature.

Keywords: PFAS, sorption, biochars, activated carbon, carbon-rich materials, modeling.

1. Introduction

Perfluoroalkyl substances (PFAS), such as perfluoroalkyl carboxylates (PFCA) and perfluoroalkane sulfonates (PFSA), have gained attention in recent years due to their high persistence in the environment, their bioaccumulation, and their toxicity. PFAS have been widely used for more than 50 years in industrial applications such as ~~in~~ fire-fighting foams, inks, lubricants, surfactants, and oil and water repellents for leather, paper and textile goods. Their strong C-F bonds contribute to their high resistance to thermal, biological and photolytic degradation, and they are found in a range of environmental matrices (Prevedouros et al., 2006).

PFAS have been detected at levels up to several mg kg^{-1} and μg L^{-1} in soils and freshwater environments respectively (Brusseau et al., 2020; Colomer-Vidal et al., 2022). They can be transferred from soil to plants through root uptake and bioaccumulate in these organisms (Lesmeister et al., 2020). PFAS can also reach groundwaters by soil run-off (Gellrich et al., 2012). Hence, remediation techniques to decrease PFAS mobility in the environment are ~~of~~ attracting increasing attention. In this regard, activated carbon has been shown to be an effective sorbent for PFAS removal from residual waters (Ochoa-Herrera and Sierra-Alvarez, 2008; Qian et al., 2017), and is occasionally tested in the laboratory to remediate contaminated soils (Kupryianchyk et al., 2016). Biochars are a sustainable alternative to activated carbon, given their similar sorption properties towards organic pollutants (Ahmad et al., 2014), and they may be considered a cost-effective alternative for soil remediation (Silvani et al., 2019; Askeland et al., 2020; Sørmo et al., 2021). Additionally, other organic byproducts such as charcoal-based materials rejected by the steel industry and compost have been reported to be capable of sorbing PFAS (Sörengård et al., 2020).

It has been suggested that sorbent properties such as surface area and surface chemistry may play important roles in PFAS sorption in activated carbons (Saeidi et al., 2020a). Furthermore, PFAS sorption generally increases with greater fluorinated chain length

(Sörengård et al., 2020). Other factors such as pH, ionic strength and dissolved organic carbon (DOC) levels can also modify sorption in activated carbons (Saeidi et al., 2020a; Xiao et al., 2017; Yu et al., 2012). However, new systematic studies are required to evaluate the role of different factors governing PFAS sorption in biochars of contrasted properties, as well as to obtain sorption parameters for PFAS with different chain lengths in other carbon-rich materials such as compost and charcoal fines. The current literature on PFAS sorption by carbon-rich materials mainly focuses on the evaluation of the maximum loading capacities of the materials, aiming to determine their efficiency in the context of wastewater remediation (Zhang et al., 2020). The estimation of the solid-liquid distribution coefficient (K_d) may be a suitable parameter to assess the sorption affinity of PFAS for a given material, helping to assess its potential remediation effectiveness. However, descriptions in the literature of K_d prediction models for PFAS sorption by these carbon-rich sorbents are scarce.

In this study, sorption kinetics, sorption isotherms and the effects of pH, calcium concentration and DOC content on PFAS sorption by carbon-rich materials (including biochars, compost, charcoal fines and activated carbon) were assessed. Additionally, K_d values were derived for PFCA and PFSA that contained fluorinated carbons ranging from 4 to 11, in a set of ten carbon-rich materials. The key sorbent properties affecting PFAS sorption were identified by principal component analysis (PCA), and, along with PFAS chain length, formed the basis for the development of a multivariate linear K_d prediction model. The model applied robust stepwise multiple linear regression and was validated using external sorption data gathered from the literature. The aim was to see whether it might help to identify the most promising carbon-rich materials for the remediation of areas contaminated with PFAS.

2. Materials and methods

2.1. Reagents and PFAS standards

Milli-Q double deionized water (18.2 MΩ cm-1) was obtained from a water purification system (USF PureLaB Plus, Spain). HPLC-grade acetonitrile (≥ 99.9%) as well as extra pure sodium azide (≥ 99.0%) and calcium chloride dihydrate (99%) were purchased from Merck (Germany), while ammonium acetate (96%) was obtained from Panreac (Spain). Analytical standards of perfluorohexanoic acid (PFHxA; 97%), perfluorooctanoic acid (PFOA; 96%), perfluorononanoic acid (PFNA; 97%), perfluorododecanoic acid (PFDoA; 95%) and potassium perfluorohexanesulfonate (PFHxS; 98%) were obtained from Sigma-Aldrich (Germany). Tetrabutylammonium perfluorobutanesulfonate (PFBS; 98%) and tetrabutylammonium perfluorooctanesulfonate (PFOS; 95%) were purchased from Fluka (Austria). The physicochemical properties of the PFAS are summarized in Table S1 in the Supplementary Information, including those used to test the model developed.

Individual PFAS stock solutions of 1 g L^{-1} were prepared in acetonitrile, while the working solutions for the sorption experiments were prepared by the dilution of the stock standards in acetonitrile. Isotopically labelled standard solutions of sodium perfluoro-1-[1,2,3,4,-$^{13}C_4$]-octanesulfonate (MPFOS) and perfluoro-n-[1,2,3,4,-$^{13}C_4$]-octanoic acid (MPFOA), both at concentrations of 50 μg mL^{-1} in methanol, were purchased from Wellington Laboratories (Canada). Working standard solutions of both MPFOS and MPFOA were prepared at 500 ng mL^{-1} of each PFAS in acetonitrile. All solutions were stored at 5°C in glass vials with polyethylene caps (Sigma-Aldrich, Germany).

Based on the pK_a values reported in Table S1, all the PFAS were expected to be in their anionic form in the experimental conditions of the sorption tests. The PFAS chain length in this study refers to the total number of fluorinated carbons in the alkyl chain (CF_2), including the final $–CF_3$ moiety.

100 *2.2. Materials*

101 Six biochar, one coal fines, one compost and two activated carbon samples were
102 examined. Biochar obtained from tree barks (TB) was provided by a wine factory after
103 pyrolyzing the feedstock under a nitrogen atmosphere at 400ºC for 3 hours, while biochars from
104 crop eucalyptus (CE), sugarcane bagasse (SB), castor meal (CM), coconut pericarp (CP) and
105 water hyacinth (WH) were obtained after pyrolyzing each feedstock at 350ºC for 70 minutes as
106 described elsewhere (Doumer et al., 2015). The coal fines (CF) sample was provided by a
107 Brazilian metallurgical company, while municipal organic waste (MOW) compost was
108 provided by a waste management treatment plant in Barcelona (Spain). The initial carbon-rich
109 bulk samples weighing a few kg were sieved at < 2 mm. The sample mass was homogenized
110 and representatively reduced using riffle splitters before sorption tests. Two granular activated
111 charcoals, GAC (C2889) and NGAC (Norit® 1240W), were purchased from Sigma-Aldrich
112 (Steinheim, Germany). All materials were tested without any further treatment. The main
113 physicochemical properties of the materials are summarized in Table 1, while the
114 characterization methods are summarized in Section S1 of the Supplementary Information.

115 *2.3. Sorption experiments*

116 Two biochars (TB and CE), a compost sample (MOW) and a charcoal fines sample (CF)
117 were selected to assess PFAS sorption kinetics, sorption isotherms and the effects of pH,
118 calcium concentration and DOC content on sorption. TB and CE were selected because their
119 physicochemical properties are different from those of other reported biochars (Fagbayigbo et
120 al., 2017; Guo et al., 2017); for their part, the evaluation of compost and charcoal fines has
121 barely been studied in the literature. Additionally, the NGAC sample was used to compare the
122 sorption isotherms obtained by the other selected materials. PFOS was selected as the PFAS
123 representative. Once the equilibration time and initial concentrations were optimized, sorption
124 experiments of 7 PFAS (see Table S1) were performed in the 10 carbon-rich materials.

To run all the sorption experiments (OECD, 2000), one gram of dried material was introduced into 80-mL polypropylene centrifuge tubes before the addition of 25 mL of a 0.1% w/w NaN_3 solution (pH 7.7 unless specified otherwise). The resulting suspension was shaken in an end-over-end shaker at 30 rpm and room temperature (18-20ºC) for 16 h to obtain a pre-equilibrium state between the solid material and the solution. Selected volumes of individual PFAS working solutions were then added to the suspensions to achieve a given initial concentration. All experiments were run in triplicate.

For the sorption kinetics, PFOS was spiked at 400 ng mL^{-1}, while the initial concentrations for PFOS sorption isotherms ranged from 10 to 600 ng mL^{-1} for TB, CE, MOW and CF, and 500 to 10,000 ng mL^{-1} for NGAC, as higher sorption coefficients were expected for this charcoal. The pH of all the resulting experiments did not differ (± 0.2) from the initial sample pH reported in Table 1. For the evaluation of the effects of pH and calcium concentration, specific contact solutions were adjusted according to previous acid/base tests using 0.5 N HCl and 0.5 N NaOH to achieve a final suspension pH of 5, 7 or 11 after the pre-equilibration step, with the final volume being 25 mL. For each pH, several compositions of the contact solutions were tested. These solutions contained NaN_3 at 0.1% and calcium at a natural concentration, 10 mM or 100 mM. The suspensions were spiked with 400 ng mL^{-1} of PFOS after the pre-equilibration step, and the DOC content in the supernatants of these experiments was also monitored.

For the remaining PFAS, sorption experiments were conducted to derive K_d values at a single spiking concentration (see Table S2). In view of the results from the PFOS sorption isotherms in the five representative materials, it was assumed that the derived K_d values were within the linear range of PFAS sorption. In all the experiments, after each individual PFAS spike, tubes were shaken at 30 rpm for 48 hours and centrifuged for 30 min at 10ºC and 7800 *g*

149 (AJ2-HS, Beckman Coulter, USA). After centrifugation, the supernatants were removed using
150 a plastic syringe, passed through 0.45-µm filters and stored at 4ºC in glass vials until analysis.
151 *2.4. Quality control*
152 The relative standard deviation between the replicates was generally lower than 15%,
153 but rose to 30% in a few worst-case scenarios. Quality control of the analyses included blank
154 samples that were tested using the same procedure described in 2.3, but without PFAS spiking,
155 to test for the presence of PFAS in the samples. In addition, aqueous control samples with a
156 PFAS concentration representative of the tested concentration range were assayed to quantify
157 PFAS losses during the experimental stages of the batch test. Results from the analyses of the
158 blanks showed that no PFAS were present in the samples prior to the analysis. Regarding the
159 aqueous control samples, negligible losses were observed for all PFAS except for PFDoA, of
160 which only 40% was recovered. The results were corrected accordingly (Fabregat-Palau et al.,
161 2021).
162 *2.5. PFAS analysis by LC-MS/MS*
163 To quantify the PFAS after the sorption experiments, a 750-µL aliquot of the
164 supernatant was transferred to a 2-mL chromatography vial. 10 µL of the MPFOS and MPFOA
165 internal standard working solution and 240 µL of acetonitrile were added to the vial to obtain a
166 final volume of 1 mL. The PFAS were subsequently analyzed by liquid chromatography-
167 tandem mass spectrometry (LC-MS/MS). Details of the chromatography methods can be found
168 elsewhere (Fabregat-Palau et al., 2021).
169 *2.6. Data treatment*
170 The sorption solid-liquid distribution coefficient, K_d (mL g^{-1}), was calculated as the ratio
171 of the concentration of the target PFAS sorbed into the solid phase, C_s (ng g^{-1}), to the
172 concentration in the aqueous phase at equilibrium, C_{eq} (ng mL^{-1}):

$$K_d = \frac{C_s}{C_{eq}} \quad (1)$$

C_{eq} values were directly determined by LC-MS/MS, whereas C_s was calculated with the following equation:

$$C_s = \frac{(C_{in} - C_{eq}) \cdot V}{m} \quad (2)$$

where C_{in} (ng mL^{-1}) corresponds to the initial concentration of PFAS added to the suspension, V (mL) is the volume of solution and m (g) refers to the dry mass of the material. The sorption yield, S (%), was calculated as follows:

$$S\,(\%) = \frac{(C_{in} - C_{eq})}{C_{in}} \cdot 100 \quad (3)$$

The kinetic data were fitted to the pseudo-second-order model (PSOM):

$$\frac{t}{C_{s,t}} = \frac{1}{K_2\, C_{s,eq}^2} + \frac{t}{C_{s,eq}} = \frac{1}{V_0} + \frac{t}{C_{s,eq}} \quad (4)$$

where $C_{s,t}$ (ng g^{-1}) is the sorbed concentration at time *t*, K_2 (g ng^{-1} h^{-1}) is the PSOM rate constant, $C_{s,eq}$ (ng g^{-1}) is the sorbed concentration at equilibrium and V_0 is the initial sorption rate (ng g^{-1} h^{-1}) (Yu et al., 2009).

Both the kinetic and isotherm data were fitted using the least-squares method (cftoolbox, Matlab® R2009a (MathWorks Inc., USA)). Fisher's least significant difference (FLSD) test was run, using Statgraphics Centurion 18.1.14 (Statgraphics Technologies, USA) and log_{10}-transformed data. To identify the key sorbent properties affecting PFAS sorption, a principal component analysis (PCA) was performed (PLS Toolbox 703, Matlab® R2009a (MathWorks Inc., USA)) after autoscaling and performing a log_{10} transformation of the data (with the exception of pH, pH_{PZC} and log K_{OW}).

190 *2.7. Model construction*

191 The K_d prediction model was constructed using a calibration set based on our 70 own
192 experimental K_d data in addition to 15 additional literature entries (Deng et al., 2015; Xiao et
193 al., 2017; Siriwardena et al., 2019) selected to enlarge the range values of the relevant properties
194 used as model variables. These additional entries also improved the distribution of the K_d values
195 along the calibration set, regardless of the type of material. Additional data gathered from the
196 literature were used as a validation set (Table S3). The criteria for including literature data were:
197 (i) data must originate from batch experiments with PFAS and carbon-rich sorbents with
198 experimental conditions similar to OECD 106 test (OECD, 2000); (ii) tested materials should
199 be similar to those used in our work, such as biochars or activated carbons, but excluding data
200 derived from studies using modified/doped materials or material mixtures (*i.e.*, soil + biochar);
201 (iii) the characterization data of the sorbents must be available; (iv) the K_d values for the PFAS
202 should be reported or be derivable from the information reported in the study, resulting in K_d
203 values within the linear sorption range.

204 The model was constructed by stepwise multiple linear regressions (SMLR), and the
205 least squares of the regressions were iteratively weighted with a bisquare weighting function to
206 avoid the potential skewness provoked by data in the calibration set. Once the model was built
207 up, it was tested against the validation dataset, which included the sorption K_d data from
208 biochars and activated carbon for both PFCA and PFSA with a fluorinated alkyl chain number
209 ranging from 3 to 8. The total number of accepted entries of the validation set was 46 (15 for
210 biochars and 31 for activated carbons). The predictive quality of the model was statistically
211 evaluated as described in section S2 of the Supplementary Information.

3. Results and discussion

3.1. Physicochemical properties of the samples

The total carbon content (%TC) of the biochars ranged from 27 to 80%. The presence of inorganic carbon species was minor (< 1-7%) according to the differences between C_{ORG} and TC. The C_{ORG} differed among the biochars obtained under the same pyrolysis conditions due to differences in the feedstocks (Doumer et al., 2015). The C_{ORG}/O molar ratio of the biochar and compost samples ranged from 1.3 to 8.6 and correlated well ($r^2 = 0.91$, $p < 0.001$, $n = 7$) with the percentages of aromatic carbon revealed by ^{13}C-NMR (Doumer et al., 2016; Venegas et al., 2015). Therefore, this parameter was chosen as a good indicator of the aromaticity of the material. The median particle size distribution of the samples ranged from 40 to 1010 µm (see Figure S1). With the exception of TB, the specific surface area (SSA) of the biochars was ≤ 3 m^2 g^{-1}. Despite the low surface area of some of these sorbent materials, SEM images revealed a relatively well-developed porous structure (see Figure S2). By contrast, the commercial GAC and NGAC samples presented both developed porosity and a high SSA.

The pH and pH_{PZC} of the samples ranged from 6 to 10 and 5 to 11 respectively. Since pH_{PZC} is defined as the pH at which the material presents a net neutral charge, positively-charged surfaces may be expected for pH_{PZC} > pH, whereas negatively-charged surfaces may be expected for pH_{PZC} < pH. Therefore, although high ash contents may influence pH_{PZC}, the difference between pH_{PZC} and pH was considered a qualitative indicator of the overall bulk net surface charge. The main water-soluble cation and anion levels in the blank samples are reported in Table S4. With the exception of TB, the DOC content of the biochars was relatively high (> 100 mg L^{-1}). These high DOC contents, which may be attributed to the presence of unpyrolyzed carbon species, were confirmed by the FTIR bands at 2860 and 2930 cm^{-1} (Figure S3) that were related to symmetric and asymmetric aliphatic C-H stretch vibrations, respectively.

3.2. Effect of equilibration time on PFOS sorption

The evaluation of the sorption kinetics of PFOS in the four tested materials revealed that equilibrium was reached within the first 12-24 hours (Figure 1), except for MOW, which required longer times. Thus, the sorption experiments were carried out for 48 hours, in agreement with previous kinetic studies evaluating PFOS sorption in biochars with contrasting properties (Guo et al., 2017). The kinetic data were fitted to a PSOM, obtaining Pearson correlation coefficients close to 1 (Table S5). The PSOM results confirmed that PFOS sorption was faster in biochars than in compost and charcoal fines, although MOW showed a stronger affinity at longer times than the CE biochar.

3.3. Effect of initial PFOS concentration on PFOS sorption

Sorption isotherm plots (C_s vs C_{eq} plots) were constructed to evaluate the effect of the initial PFOS concentration on K_d (Figure 2). Whereas previous reports ~~of~~ have indicated saturated PFOS sorption in biochar and activated carbon samples at mg L^{-1} levels (Guo et al., 2017; Ochoa-Herrera and Sierra-Alvarez, 2008), and also close-to-linear isotherms for PFOS on activated carbon (Zhang et al., 2016), linear sorption isotherms were obtained under our experimental conditions ($r^2 > 0.97$) for all the tested materials. This could be attributed to both the higher solid/liquid ratio (40 g L^{-1}) and the lower initial PFOS concentration used in our experiments, providing a sufficient amount of sorption sites for the PFAS and, thus, ensuring a linear sorption pattern.

3.4. Effects of pH, Ca concentration and DOC content on PFOS sorption

The sorption percentages of PFOS under different experimental conditions are shown in Figure 3. For a given Ca concentration, PFOS sorption generally decreased with increasing pH, in agreement with previous findings (Saeidi et al., 2020a). This may be partly due to the increasing number of repulsions between the negatively-charged surface and the PFAS at increasing pH values. This decrease was more significant between pH 5 and pH 7 for the CE

and CF materials, which had the lowest pH_{PZC}, highlighting the importance of the chemical groups present at the material surface for PFAS sorption (Saeidi et al., 2020a). The sorption percentages under acidic conditions for each material were high and relatively constant, regardless of the calcium concentration, whereas at neutral and, especially, at alkaline pH values the sorption percentages increased with the Ca concentration. This might be attributed to two complementary mechanisms: the shielding effect of calcium ions under alkaline conditions that reduces the negative repulsions between the PFAS and the material surface, and the presence of electrostatic bridge interactions between the negatively-charged surface and PFOS assisted by divalent cations (Du et al., 2014).

It has been reported that DOC negatively affects PFOS sorption in activated carbons at levels over 10 mg C L^{-1} (Yu et al., 2012), which may be explained by the competition between DOC and the PFAS for the solid material; however, other authors have attributed it to the blocking effect of DOC on the sorption sites present in the microporosity (Saeidi et al., 2020b). For our materials, the DOC contents ranged from 10 to 250 mg C L^{-1} under acidic and neutral conditions depending on the material and regardless of the calcium concentration, although these levels increased significantly up to 1100 mg C L^{-1} under alkaline conditions and low ionic strength conditions for some materials such as MOW (Figure 3). The DOC content was reduced under acidic conditions, probably due to the protonation of the carboxyl and alkoxy functional groups present at the surface of the materials. Under alkaline conditions, such acidic functional groups were deprotonated, thus increasing the solubility of the organic compounds and leading to an increase in the DOC level. An increase in ionic strength reduced the DOC content by decreasing DOC solubility and promoting organic matter flocculation. Therefore, according to the DOC contents in our experiments, a sorption inhibition was anticipated in certain scenarios due to the increasing concentration of DOC. At the highest Ca concentration, the DOC content remained low and much less dependent on pH, whereas a decrease in PFOS sorption

287 percentages with pH could be partially explained by increasing DOC content for a given Ca
288 concentration.

289 *3.5. Sorption of PFAS with different chain lengths*

290 Since the K_d of PFOS was constant at the concentration ranges tested, further
291 experiments aiming to calculate the sorption parameters for other PFAS were carried out at a
292 single spiking concentration, ensuring the quantification of K_d within the linear sorption range.

293 The results of these experiments are shown in Table 2. PFBS, PFHxA and PFHxS had
294 K_d values up to 50 L kg^{-1} in the compost, charcoal fines and most biochar samples, although
295 they eventually increased to 115 L kg^{-1} in the biochar TB. On the other hand, K_d values for
296 PFOA, PFOS and PFNA were higher than those of the previous short-chained PFAS (up to 145
297 L kg^{-1}) and increased to 2,900 L kg^{-1} in the biochar TB. PFDoA was the PFAS with the highest
298 K_d values, which ranged from 190 to 1,800 L kg^{-1} for all materials except TB, for which K_d
299 value was above the 10^4 L kg^{-1} range. This suggests a moderate to high affinity between PFDoA
300 and most carbon-rich materials. The K_d values for all PFAS in the two activated carbon samples
301 were much higher than for the rest of materials (up to four orders of magnitude higher).
302 Specifically, K_d values in these materials ranged from 14,000 to 480,000 L kg^{-1} and indicated
303 a very high PFAS sorption affinity. Moreover, the FLSD test revealed that the sorption of PFAS
304 for a given material increased with greater PFAS chain length, in agreement with previous
305 findings (Sörengård et al., 2020; Xiao et al., 2017).

306 *3.6. Multivariate analyses between material properties and PFAS sorption parameters*

307 To better identify the key sorbent properties affecting PFAS sorption in carbon-rich
308 materials, a PCA was performed with the data obtained in our experiments (Table 2) and
309 material properties (Figure 4). Using two principal components, 70% of the data variance was
310 explained (47% and 23% by the first and second principal component respectively). According
311 to the relative positions of the loading variables in the first two principal components, the

312 C_{ORG}/O molar ratio, which may be related to the aromaticity of the material, had a positive
313 effect on K_d. This agrees with previous findings that the basic sites in π-electron-rich regions
314 in carbon-rich materials are important for PFAS sorption (Saeidi et al., 2020a). Unlike soils, in
315 which the C_{ORG} content is the main parameter governing sorption (Fabregat-Palau et al., 2021),
316 our PCA data indicated that C_{ORG} content alone did not seem to have a major effect on the K_d
317 of PFAS in carbon-rich materials. Instead, the C_{ORG}/O molar ratio seemed to be a better
318 descriptor of PFAS sorption, likely due to the hydrophobic interactions (Li et al., 2019).
319 Additionally, a higher C_{ORG}/O ratio indicates a lower amount of functional groups able to repel
320 PFAS due to negative electrostatic repulsions. The SSA (with all values originating from N_2-
321 BET measurements) also had a positive effect on K_d in the PCA, in agreement with previous
322 findings (Saeidi et al., 2020a). As the SSA is affected by both particle size distribution and
323 porosity, this parameter may be considered an indicator of the number of sorption sites that can
324 interact with PFAS. According to the PFAS molecular size (150 – 300 cm^3 mol^{-1}, Kim et al.,
325 2015) and the pore width of the sorbents (Table 1), all PFAS molecules were expected to have
326 access to the micropore structure.

327 As discussed in section 3.4, PFAS sorption is favored when pH < pH_{PZC}. According to
328 our PCA results, the difference between pH_{PZC} and pH had a positive influence on K_d. This may
329 be explained by the presence of interaction mechanisms such as electrostatic interactions or
330 hydrogen bonding in the case of positively-charged surfaces (Du et al., 2014), thus highlighting
331 the additional influence of polar surface functional groups on PFAS sorption (Saeidi et al.,
332 2020a). Neither the cation exchange capacity (CEC) nor the ash content had a direct effect on
333 K_d. However, DOC content had a negative effect on K_d, as previously discussed in section 3.
334 ~~3~~4. Despite the influence of ionic strength, as discussed in section 3.4, water-soluble cations
335 did not have a significant influence on K_d according to our PCA data. This suggests that
336 although shielding repulsions and/or cation bridge interactions may play a role in PFAS

sorption under certain experimental conditions for a single material (Du et al., 2014), these interactions are, overall, not predominant when all the materials are considered. Similarly, although it has been suggested that anion exchange interactions may play a role in PFAS sorption in activated carbons (Saeidi et al., 2020a), our PCA results showed that water-soluble anions did not have a direct effect on K_d.

Adding a third principal component to the PCA explained an additional 11% of the data variance, which mostly accounted for the contribution of PFAS hydrophobicity, represented by its log K_{OW}. Similar results were obtained by evaluating PFAS hydrophobicity with its number of CF_2. These findings agree with the increase in sorption observed in section 3.5 with greater PFAS chain length, which might be due to the stronger binding of long-chained PFAS to carbon-rich materials through hydrophobic interactions (Li et al., 2019).

3.7. Development of a prediction model

A simple linear model was developed to predict K_d using specific physicochemical properties of the PFAS and the carbon-rich materials. The significant sorbent properties affecting PFAS sorption previously identified with the PCA (C_{ORG}/O molar ratio, SSA, log K_{OW}, (pH_{PZC} – pH) and DOC) were considered. As shown in Table S1, the hydrophobicity of the PFAS, expressed as log K_{OW}, increased linearly with each fluorinated carbon added to the alkyl chain (log $K_{OW} = 0.75 (\pm 0.07) \times$ number of CF_2, $r^2 = 0.98$, $p < 0.001$, $n = 15$). Due to this strong correlation, PFAS hydrophobicity could be reasonably evaluated based on either the number of CF_2 or the log K_{OW}. In principle, K_{OW} values differentiate better between PFAS that have the same number of CF_2 but different functional groups (e.g., PFOS and PFNA). However, and although all log K_{OW} values. in Table S1 were calculated values, they may differ from those obtained experimentally. Therefore, CF_2, an easily obtainable parameter that is descriptive of PFAS, was chosen as the descriptor for hydrophobicity in the development of the prediction model.

Because of the low number of studies in the literature reporting DOC levels, DOC content was excluded from the model. Subsequently, robust SMLR with the 85 entries of the calibration set was performed after a $\log_{10}$ transformation of the data (with the exception of CF_2, pH_{PZC} and pH). By considering only the C_{ORG}/O molar ratio, SSA and CF_2 90% of the K_d (PFAS) data variance was explained. The inclusion of the variable (pH_{PZC} – pH) resulted in a non-significant coefficient and did not increase the explained variance, and therefore was excluded from the model (also because pH_{PZC} may be affected for some materials with high ash contents). Accordingly, the final model included the C_{ORG}/O molar ratio and SSA, which may be indicative, respectively, of the quality and quantity of the sorption sites available for PFAS sorption through hydrophobic interactions. In addition, the inclusion of the variable CF_2 made the model applicable to a wide range of PFAS.

The robust SMLR resulted in the following equation that defined the prediction model:

$$\log K_d = 1.87\ (\pm 0.39) \log C_{ORG}/O + 0.49\ (\pm 0.14) \log SSA + 0.25\ (\pm 0.06)\ CF_2 - 0.94\ (\pm 0.46) \quad (7)$$

$r^2 = 0.90$, $n = 85$; $p < 0.001$

The range of values of the model variables included in the calibration set helps to establish the application range of the K_d (PFAS) prediction model. Specifically, the C_{ORG}/O molar ratio ranged from 1.3 – 104, SSA (measured in all cases by N_2-BET) ranged from 0.06 – 2,450 $m^2\ g^{-1}$, and PFAS chain length ranged from 3 – 11 CF_2 units. Although not included in the prediction model, the sample pH in the calibration set ranged from 4 – 10, which suggests that the prediction model may be applicable to a wide range of environmentally relevant pH values. According to the expected PFAS maximum sorption capacities of carbon-rich products (up to a hundred g kg^{-1} for biochars and several hundreds g kg^{-1} for activated carbons, Gagliano et al., 2020), and PFAS concentrations found in fresh- and groundwaters of impacterd sites (up to 300 µg L^{-1}, Colomer-Vidal et al., 2022; McGuire et al., 2014) the model should be applicable to most environmental conditions, since materials are not likely to reach saturation and,

385 therefore, sorption will fall within the linear range of the isotherms, thus being K_d a good
386 descriptor of the sorption process.

387 *3.8. External validation of the prediction model*

388 The K_d (PFAS) prediction model was externally validated with the validation set by
389 splitting the data into two sets according to the type of materials (biochars and activated
390 carbons), as shown in Figure 5. A satisfactory prediction was obtained in both cases, generating
391 a slope between predicted and experimental log K_d values that was statistically equal to one and
392 a null y-intercept, as well as explaining 75% and 68% of the data variance respectively.
393 According to the root square mean error (RMSE) and residual predictive deviation (RPD)
394 values, the quality of the model for predicting PFAS K_d values in both biochars and activated
395 carbons was acceptable, especially considering that the validation dataset was affected by
396 different sources of uncertainty, including the intrinsic variability of the literature data and the
397 fact that K_d values were derived from different sorption parameters. The residuals were mostly
398 around 0.5 log K_d units, increasing to 1.2 log K_d units in the worst-case scenario, which is
399 acceptable taking into account the variability of the validation dataset and the fact that the model
400 aims to roughly group materials according to their PFAS sorption affinity which may vary over
401 six orders of magnitude. The external validation of the model considering the overall dataset
402 without refining data among materials also generated a satisfactory prediction, generating a
403 slope between predicted and experimental logK_d that was statistically equal to one (0.94 ± 0.19)
404 and a null y-intercept, as well as explaining 71% of the variance, and obtaining RMSE and RPD
405 values of 0.53 and 1.57. All these results suggest that the log K_d values of PFAS for carbon-
406 rich materials can be approximately predicted with acceptable accuracy using easily-derived
407 physicochemical properties of the sorbent and PFAS descriptors of hydrophobic interactions,
408 highlighting the minor role of electrostatic interactions in the PFAS sorption by carbon-rich
409 materials.

4. Conclusions

The sorption of anionic PFAS by carbon-rich materials (biochars, activated carbon, compost and charcoal fines), although affected by solution-specific properties (such as pH, the concentration of divalent cations and DOC content), was mainly controlled by hydrophobic interactions. According to the proposed model, K_d values for PFAS in carbon-rich materials can be predicted with acceptable accuracy using only a few physicochemical properties of the sorbent (C_{ORG}/O molar ratio and SSA) and the PFAS (number of CF_2). The successful external validation of the proposed model using literature data, although affected by intrinsic sources of variability, suggests that the model may be useful in assessing the potential affinity of carbon-rich materials for PFAS in the early screening of candidate materials for environmental remediation. However, additional sorption data of PFAS of different chain-length in extensively characterized carbon-rich materials will help to further improve the application range of the model. In addition, the identification of key sorbent properties affecting PFAS sorption may be useful in optimizing industrial processes (i.e., pyrolysis/composting conditions or physicochemical activation methods) to magnify these properties in order to increase sorbent affinity.

Acknowledgements

This work was supported by the Ministerio de Ciencia e Innovación de España (PID2020-114551RB-I00) and the Generalitat de Catalunya (2017 SGR 907).

References

Ahmad, M., Rajapaksha, U. A., Lim, J. E., Zhang, M., Bolan, N., Mohan, D., Vithanage, M., Lee, S. S., Ok, Y. S., 2014. Biochar as a sorbent for contaminant management in soil and water: A review. Chemosphere, 99, 19–33. https://doi.org/10.1016/j.chemosphere.2013.10.071

Askeland, M., Clarke, B. O., Cheema, S. A., Mendez, A., Gasco, G., Paz-Ferreiro, J., 2020. Biochar sorption of PFOS, PFOA, PFHxS and PFHxA in two soils with contrasting texture. Chemosphere, 249, 126072. https://doi.org/10.1016/j.chemosphere.2020.126072

Brusseau, M. L., Anderson, R. H., Guo, B., 2020. PFAS concentrations in soils: Background levels versus contaminated sites. Sci. Total Environ. 740, 140017. https://doi.org/10.1016/j.scitotenv.2020.140017

Colomer-Vidal, P., Jiang, L., Mei, W., Luo, C., Lacorte, S., Rigol, A., Zhang, G., 2022. Plant uptake of perfluoroalkyl substances in freshwater environments (Dongzhulong and Xiaoqing Rivers, China). J. Hazard. Mater. 421, 126768. https://doi.org/10.1016/j.jhazmat.2021.126768

Deng, S., Nie, Y., Du, Z., Huang, Q., Meng, P., Wang, B., Huang, J., Yu, G., 2015. Enhanced adsorption of perfluorooctane sulfonate and perfluorooctanoate by bamboo-derived granular activated carbon. J. Hazard. Mater. 282, 150–157. https://doi.org/10.1016/j.jhazmat.2014.03.045

Doumer, M. E., Rigol, A., Vidal, M., Mangrich, A. S., 2016. Removal of Cd, Cu, Pb, and Zn from aqueous solutions by biochars. Environ. Sci. Pollut. R. 23 (3), 2684–2692. https://doi.org/10.1007/s11356-015-5486-3

Doumer, M. E., M., Arízaga, G. G. C., da Silva, D. A., Yamamoto, C. I., Novotny, E. H., Santos, J. M., dos Santos, L. O., Wisniewski Jr, A., de Andrade, J. B., Mangrich, A. S., 2015. J Slow pyrolysis of different Brazilian waste biomasses as sources of soil conditioners and

energy, and for environmental protection. J. Anal. Appl. Pyrol. 113, 434–443. https://doi.org/10.1016/j.jaap.2015.03.006

Du, Z., Deng, S., Bei, Y., Huang, Q., Wang, B., 2014. Adsorption behavior and mechanism of perfluorinated compounds on various adsorbents — A review. J. Hazard. Mater. 274, 443–454. https://doi.org/10.1016/j.jhazmat.2014.04.038

Fabregat-Palau, J., Vidal, M., Rigol, A., 2021. Modelling the sorption behaviour of perfluoroalkyl carboxylates and perfluoroalkane sulfonates in soils. Sci. Total Environ. 801. https://doi.org/10.1016/j.scitotenv.2021.149343

Fagbayigbo, B. O., Opeolu, B. O., Fatoki, O. S., Akenga, T. A., Olatunji, O. S., 2017. Removal of PFOA and PFOS from aqueous solutions using activated carbon produced from Vitis vinifera leaf litter. Environ. Sci. Pollut. R. 24 (14), 13107–13120. https://doi.org/10.1007/s11356-017-8912-x

Gagliano, E., Massimiliano, S., Falciglia, P. P., Vagliasindi, F. G. A., Roccaro, P., 2020. Removal of poly- and perfluoroalkyl substances (PFAS) from water by adsorption: Role of PFAS chain length, effect of organic matter and challenges in adsorbent regeneration. Water Res. 171, 115381. https://doi.org/10.1016/j.watres.2019.115381

Gellrich, V., Stahl, T., Knepper, T. P., 2012. Behavior of perfluorinated compounds in soils during leaching experiments. Chemosphere, 87 (9), 1052–1056. https://doi.org/10.1016/j.chemosphere.2012.02.011

Guo, W., Huo, S., Feng, J., Lu, X., 2017. Adsorption of perfluorooctane sulfonate (PFOS) on corn straw-derived biochar prepared at different pyrolytic temperatures. J. Taiwan Inst. Chem. E. *78*, 265–271. https://doi.org/10.1016/j.jtice.2017.06.013

Kim, M., Li, L. Y., Grace, J. R., Yue, C., 2015. Selecting reliable physicochemical properties of perfluoroalkyl and polyfluoroalkyl substances (PFASs) based on molecular descriptors. Environ. Pollut. 196, 462 - 472. 462–472. https://doi.org/10.1016/j.envpol.2014.11.008

480 Kupryianchyk, D., Hale, S. E., Breedveld, G. D., Cornelissen, G., 2016. Treatment of sites
481 contaminated with perfluorinated compounds using biochar amendment. Chemosphere,
482 142, 35–40. https://doi.org/10.1016/j.chemosphere.2015.04.085
483 Lesmeister, L., Lange, F. T., Breuer, J., Biegel-Engler, A., Giese, E., Scheurer, M., 2020.
484 Extending the knowledge about PFAS bioaccumulation factors for agricultural plants – A
485 review. Sci. Total Environ. 766, 142640. https://doi.org/10.1016/j.scitotenv.2020.142640
486 Li, M., Sun, F., Shang, W., Zhang, X., Dong, W., Liu, T., Pang, W., 2019. Theoretical studies
487 of perfluorochemicals (PFCs) adsorption mechanism on the carbonaceous surface.
488 Chemosphere, 235, 606–615. https://doi.org/10.1016/j.chemosphere.2019.06.191
489 McGuire, M. E., Schaefer, C., Richards, T., Backle, W. J., Field, J. A., Houtz, E., Sedlak, D.
490 L., Guelfo, J. L., Wunsch, A., Higgins, C. P., 2014. Evidence of remediation-induced
491 alteration of subsurface poly- and perfluoroalkyl substance distribution at a former
492 firefighting training are. Envrion. Sci. Technol. 48 (12), 6644-6652.
493 http://doi.org/10.1021/es5006187.
494 Ochoa-Herrera, V., Sierra-Alvarez, R., 2008. Removal of perfluorinated surfactants by sorption
495 onto granular activated carbon, zeolite and sludge. Chemosphere, 72 (10), 1588–1593.
496 https://doi.org/10.1016/j.chemosphere.2008.04.029
497 OECD, 2000. OECD 106 Adsorption - Desorption Using a Batch Equilibrium Method. OECD
498 Guideline for the Testing of Chemicals. https://doi.org/10.1787/9789264069602-en
499 Prevedouros, K., Cousins, I. T., Buck, R. C., Korzeniowski, S. H., 2006. Sources, fate and
500 transport of perfluorocarboxylates. Env. Sci. Technol. 40 (1), 32–44.
501 https://doi.org/10.1021/es0512475
502 Qian, J., Shen, M., Wang, P., Wang, C., Li, K., Liu, J., Lu, B., Tian, X., 2017. Perfluorooctane
503 sulfonate adsorption on powder activated carbon: effect of phosphate (P) competition, pH,
504 and temperature. Chemosphere, 182, 215–222.

https://doi.org/10.1016/j.chemosphere.2017.05.033

Saeidi, N., Kopinke, F. D., Georgi, A., 2020a. Understanding the effect of carbon surface chemistry on adsorption of perfluorinated alkyl substances. Chem. Eng. J. 381, 122689. https://doi.org/10.1016/j.cej.2019.122689

Saeidi, N., Kopinke, F. D., Georgi, A., 2020b. What is specific in adsorption of perfluoroalkyl acids on carbon materials? Chemosphere, 273. https://doi.org/10.1016/j.chemosphere.2020.128520

Silvani, L., Cornelissen, G., Smebye, A. B., Zhang, Y., Okkenhaug, G., Zimmerman, A. R., Thune, G., Sævarsson, H., Hale, S. E., 2019. Can biochar and designer biochar be used to remediate per- and polyfluorinated alkyl substances (PFAS) and lead and antimony contaminated soils? Sci. Total Environ. 694, 133693. https://doi.org/10.1016/j.scitotenv.2019.133693

Siriwardena, D. P., Crimi, M., Holsen, T. M., Bellona, C., Divine, C., Dickenson, E. 2019. Changes in adsorption behavior of perfluorooctanoic acid and perfluorohexanesulfonic acid through chemically-facilitated surface modification of granular activated carbon. Environ. Eng. Sci. 36 (4), 453–465. https://doi.org/10.1089/ees.2018.0319

Sörengård, M., Östblom, E., Köhler, S., Ahrens, L., 2020. Adsorption behavior of per- and polyfluoralkyl substances (PFASs) to 44 inorganic and organic sorbents and use of dyes as proxies for PFAS sorption. J. Environ. Chem. Eng. 8 (3), 103744. https://doi.org/10.1016/j.jece.2020.103744

Sørmo, E., Silvani, L., Bjerkli, N., Hagemann, N., Zimmerman, A. R., Hale, S. E., Hansen, C. B., Hartnik, T., Cornelissen, G., 2021. Stabilization of PFAS-contaminated soil with activated biochar. Sci. Total Environ. 763. https://doi.org/10.1016/j.scitotenv.2020.144034

Venegas, A., Rigol, A., Vidal, M., 2015. Viability of organic wastes and biochars as

amendments for the remediation of heavy metal-contaminated soils. Chemosphere, 119, 190–198. https://doi.org/10.1016/j.chemosphere.2014.06.009

Xiao, X., Ulrich, B. A., Chen, B., Higgins, C. P., 2017. Sorption of Poly- and Perfluoroalkyl Substances (PFASs) Relevant to Aqueous Film-Forming Foam (AFFF)-Impacted Groundwater by Biochars and Activated Carbon. Env. Sci. Technol. 51 (11), 6342–6351. https://doi.org/10.1021/acs.est.7b00970

Yu, J., Lv, L., Lan, P., Zhang, S., Pan, B., Zhang, W., 2012. Effect of effluent organic matter on the adsorption of perfluorinated compounds onto activated carbon. J. Hazard. Mater. 225–226, 99–106. https://doi.org/10.1016/j.jhazmat.2012.04.073

Yu, Q., Zhang, R., Deng, S., Huang, J., Yu, G., 2009. Sorption of perfluorooctane sulfonate and perfluorooctanoate on activated carbons and resin: Kinetic and isotherm study. Water Res. 43 (4), 1150–1158. https://doi.org/10.1016/j.watres.2008.12.001

Zhang, Q., Zhang, W. L., Liang, Y. N., 2019. Adsorption of perfluoroalkyl and polyfluoroalkyl substances (PFASs) from aqueous solution - A review. Sci. Total Environ. 694, 133606. https://doi.org/10.1016/j.scitotenv.2019.133606

546 **Table 1**. Main physicochemical properties of the sorbent materials.
547

	TB	CE	SB	WH	CM	CP	MOW	CF	GAC	NGAC
Solid phase										
TC (%)	80	70	65	45	55	65	27	50	76	79
C_{ORG} (%)	77	65	60	43	55	63	27	43	73	79
TN (%)	0.65	0.57	0.60	4.0	7.0	1.0	1.8	1.4	0.47	0.38
TH (%)	2.2	4.0	4.4	3.3	5.4	4.0	2.9	2.3	0.59	0.49
TS (%)	NQ	NQ	NQ	0.25	NQ	NQ	0.47	NQ	0.17	0.45
TO (%)	12	26	22	25	22	24	27	21	8.5	2.3
C_{ORG}/O molar ratio	8.6	3.3	3.6	2.3	3.3	3.5	1.3	2.7	12	46
pH	8.9	7.2	6.0	9.2	7.3	8.9	8.3	8.0	10.1	8.7
pH_{PZC}	9.3	6.3	5.2	9.1	6.4	5.7	9.3	7.5	10.4	10.9
(pH_{PZC} – pH)	0.4	-0.9	-0.8	0.1	-0.9	-3.2	-1.0	-0.5	0.3	2.2
Ash (%)	4.0	4.5	5.0	31	11	5.5	35	24	6.6	14
CEC ($cmol_c\ kg^{-1}$)	4.7	9.6	5.2	48	10	10	51	63	17	4.5
Median particle size (μm)	40	378	226	87	482	381	1010	386	NA	1135
SSA ($m^2\ g^{-1}$)	162	0.61	1.3	3.0	0.06	0.97	9.2	7.3	580	964
Pore width (Å)	NQ	334	246	4771	290	2203	346	300	28	22
Liquid phase										
DOC ($mg\ L^{-1}$)	8.4	185	122	827	832	125	134	13	2.7	1.9
∑ Cl^-, NO_3^-, SO_4^{2-}, PO_4^{3-} ($meq\ L^{-1}$)	0.89	3.9	0.10	60	3.6	14	11	2.2	2.2	0.10
∑ K^+, Na^+, Ca^{2+}, Mg^{2+} ($meq\ L^{-1}$)	1.5	3.6	1.2	70	5.8	8.4	12	2.3	3.6	0.20

548 NA, not analyzed; NQ, not quantifiable; TC = total carbon; C_{ORG} = organic carbon; TN = total
549 nitrogen; TH = total hydrogen; TS = total sulphur; TO = total oxygen; pH_{PZC} = pH of point zero
550 charge; CEC = cation exchange capacity; SSA = specific surface area; DOC = dissolved organic
551 carbon.

552

553 **Table 2**. K_d values of the PFAS for the 10 carbon-rich materials. Uppercase letters indicate significant differences ($p < 0.05$) among the K_d (PFAS) for a
554 given material among the PFAS tested, as determined by the FLSD test.

Material	PFBS	PFHxA	PFHxS	PFOA	PFNA	PFOS	PFDoA
TB	19 ^{A}	25 ^{A}	115 ^{B}	450 ^{C}	1.2 x 10^{3} ^{D}	2.9 x 10^{3} ^{E}	5.6 x 10^{4} ^{F}
CE	8 ^{A}	20 ^{B}	23 ^{B}	35 ^{BC}	61 ^{CD}	75 ^{D}	395 ^{E}
SB	9 ^{A}	17 ^{B}	22 ^{BC}	27 ^{C}	110 ^{D}	110 ^{D}	1.3 x 10^{3} ^{E}
WH	10 ^{A}	19 ^{B}	29 ^{C}	41 ^{D}	68 ^{E}	145 ^{F}	1.8 x 10^{3} ^{G}
CM	16 ^{A}	38 ^{B}	47 ^{BC}	53 ^{C}	74 ^{D}	89 ^{D}	185 ^{E}
CP	11 ^{A}	15 ^{AB}	20 ^{BC}	30 ^{CD}	38 ^{E}	75 ^{D}	355 ^{F}
MOW	9 ^{A}	21 ^{B}	33 ^{C}	41 ^{C}	105 ^{D}	130 ^{D}	680 ^{E}
CF	8 ^{A}	10 ^{A}	16 ^{B}	31 ^{C}	42 ^{C}	63 ^{D}	360 ^{E}
GAC	8.0 x 10^{3} ^{A}	1.6 x 10^{4} ^{B}	5.3 x 10^{4} ^{C}	1.3 x 10^{5} ^{D}	1.7 x 10^{5} ^{DE}	2.3 x 10^{5} ^{E}	1.7 x 10^{6} ^{G}
NGAC	8.9 x 10^{4} ^{A}	1.2 x 10^{5} ^{B}	1.9 x 10^{5} ^{C}	2.7 x 10^{5} ^{D}	3.2 x 10^{5} ^{DE}	4.3 x 10^{5} ^{E}	2.6 x 10^{6} ^{G}

555

Supplementary material

Examining sorption of perfluoroalkyl substances (PFAS) in biochars and other carbon-rich materials

Joel Fabregat-Palau, Miquel Vidal, Anna Rigol*

Department of Chemical Engineering and Analytical Chemistry, University of Barcelona, Martí i Franquès 1-11, 08028 Barcelona, Spain

This file includes:

* Corresponding author, email: annarigol@ub.edu

Table S1. Main physicochemical properties of target PFAS

Name	PFAS acronym	Chemical form	CAS number	Molecular weight (g mol^{-1})	Number of CF_2	log K_{ow} **	pK_a
Perfluorobutanoic acid *	PFBA	$C_4HF_7O_2$	375-22-4	214.0	3	2.3 [a]	0.4 [a]
Perfluoropentanoic acid *	PFPeA	$C_5HF_9O_2$	2706-90-3	264.1	4	2.9 [c]	n.a.
Perfluorohexanoic acid	PFHxA	$C_6HF_{11}O_2$	307-24-4	314.1	5	3.1 [a]	-0.16 [a]
Perfluoroheptanoic acid *	PFHpA	$C_7HF_{13}O_2$	375-85-9	364.1	6	3.8 [b]	n.a.
Perfluorooctanoic acid	PFOA	$C_8HF_{15}O_2$	335-67-1	414.1	7	4.6 [a, b]	-0.2 [a]
Perfluorononanoic acid	PFNA	$C_9HF_{17}O_2$	375-95-1	464.1	8	5.5 [b]	n.a.
Perfluorodecanoic acid *	PFDA	$C_{10}HF_{19}O_2$	335-76-2	514.1	9	6.4 [b]	n.a.
Perfluoroundecanoic acid *	PFUnA	$C_{11}HF_{21}O_2$	2058-94-8	564.1	10	7.4 [b]	n.a.
Perfluorododecanoic acid	PFDoA	$C_{12}HF_{23}O_2$	307-55-1	614.1	11	8.1 [c]	n.a.
Perfluoropropane sulfonic acid *	PFPrS	$C_3HF_7O_3S$	423-41-6	250.1	3	1.7 [c]	n.a.
Perfluorobutane sulfonic acid	PFBS	$C_4HF_9O_3S$	108427-52-7 [d]	300.1	4	2.7 [a]	0.14 [a]
Perfluoropentane sulfonic acid *	PFPeS	$C_5HF_{11}O_3S$	2706-91-4	350.1	5	3.0 [c]	n.a.
Perfluorohexane sulfonic acid	PFHxS	$C_6HF_{13}O_3S$	355-46-4	400.1	6	4.3 [a]	0.14 [a]
Perfluoroheptane sulfonic acid *	PFHpS	$C_7HF_{15}O_3S$	375-92-8	450.1	7	4.3 [c]	n.a.
Perfluorooctane sulfonic acid	PFOS	$C_8HF_{17}O_3S$	111873-33-7 [d]	500.1	8	5.3 [a, b]	-3.27 [a]

* Only used for model validation purposes; ** Calculated values; n.a.: not available; [a] Deng et al., 2012; [b] Kelly et al., 2009; [c] Pubchem database; [d] CAS number corresponds to the ammonium salt

Section S1. Characterization methods of the samples

Total carbon (%TC), nitrogen (%TN), hydrogen (%TH), sulphur (%TS) and oxygen (%TO) contents were determined all by elemental analysis (EA1108 CHNS-O Fisons, Thermo Fisher Scientific). The pH of the materials was measured in a 40 g L^{-1} 0.01 M $CaCl_2$ suspension after being equilibrated during 48 hours. Total organic carbon content (%C_{ORG}) was also determined by elemental analysis with previous acidification with 2 mol L^{-1} HCl. The pH of zero point charge (pH_{PZC}) was determined adding one gram of material in a 80 mL polypropylene centrifuge tube containing 40 mL of a 0.01 M NaCl solution adjusted at pH ranging 2 – 12 using 0.5 N NaOH and 0.5 N HCl. The final pH was recorded after shaking the tubes for 24 hours and the differences between the initial and final pH were used to determine pH_{PZC} (Yu et al., 2009). Ash content was determined after calcination of the samples at 750ºC during 4 hours (ASTM D3174-02). Cation exchange capacity (CEC) was determined by the barium exchange method at material initial pH (UNE-EN ISO 11260:2018). Water soluble cations and anions were extracted using a 40 g L^{-1} Milli-Q water suspension and analysed by ICP-OES (Perkin Elmer, Optima 3200RL) and anionic chromatography (Jasco 2000 Plus), respectively. Detection wavelengths (nm) and limit of quantification (mg L^{-1}) for the selected metals were: 590 nm / 0.5 mg L^{-1} for Na; 766 nm / 0.5 mg L^{-1} for K; 279 nm / 0.05 mg L^{-1} for Mg and 318 nm / 0.05 mg L^{-1} for Ca. Anionic chromatography was performed using a IC-Pak™ Anion HR (4.6 x 75 mm) column and a gluconate-borate mobile phase at a flow rate of 0.8 mL min^{-1}. Particle size distribution was determined by laser diffraction (Beakman Coulter LS 13320) using the dry method, while specific surface area (SSA) and average pore width were determined by nitrogen adsorption (TriStar 3000, Micromeritics). Dissolved organic carbon (DOC) content of the blank supernatants was measured using a DOC analyser (Analytic Jena Multi N/C 3100) with previous acidification to pH 3 using HCl. FTIR spectra of the materials was obtained by solid KBr dilution (Thermo Nicolet 5700). The surface morphology of the solid particles was examined by scanning electron microscopy (SEM, JEOL JSM 7001F) at 15 kV.

Table S2. PFAS initial concentrations (ng mL^{-1}) used in the single-point triplicate sorption experiments.

Material	PFBS	PFHxA	PFHxS	PFOA	PFNA	PFOS	PFDoA
TB	100	100	100	100	400	N.A.	500
CE	100	100	100	100	400	N.A.	500
SB	100	100	100	100	400	400	500
WH	100	100	100	100	400	400	500
CM	100	100	100	100	400	400	500
PC	100	100	100	100	400	400	500
MOW	100	100	100	100	400	N.A.	500
CF	100	100	100	100	400	N.A.	500
GAC	2000	2000	2500	2500	4500	4500	5000
NGAC	2000	2000	2500	2500	4000	N.A.	5000

N.A.: Non Analysed (K_d data was derived from the isotherm experiments)

Table S3. List of references used to build up the validation dataset

Material information (number of samples)	Target PFAS	Number of entries	Reference
Activated Carbons			
Synthetic magnetic Activated Carbon (1)	**PFCA:** PFOA; **PFSA:** PFBS, PFHxS, PFOS	4	(Meng et al., 2019)
Commercial Active Carbon (Filtrasorb 300 *) (1)	**PFSA:** PFOS	1	(Steigerwald and Ray, 2021)
Commercial Activated Carbon (Filtrasorb 400 **) (1)	**PFCA:** PFOA; **PFSA:** PFOS	2	(Yao et al., 2014)
Commercial Activated Carbon (Filtrasorb 400 **) (1)	**PFCA:** PFPeA, PFHpA, PFOA **PFSA:** PFPeS, PFHxS, PFHpS, PFOS	7	(Yan et al., 2020)
Commercial Activated Carbon (Filtrasorb 400 **) (1)	**PFSA:** PFOS	1	(Senevirathna et al., 2010)
Commercial Activated Carbon (Filtrasorb 400 **) (1)	**PFCA:** PFOA; **PFSA:** PFBS, PFOS	3	(Ochoa-Herrera et al., 2008)
Commercial Activated Carbon (Filtrasorb 400 **) (1)	**PFSA:** PFBS, PFOS	2	(Carter and Farrell, 2010)
Commercial Activated Carbon (NORIT ® 1240W ***) (1)	**PFCA:** PFBA, PFPeA, PFHxA, PFHpA, PFOA, PFNA **PFSA:** PFBS, PFHxS	8	(Stebel et al., 2019)
Commercial Activated Carbon (1)	**PFCA:** PFOA; **PFSA:** PFOS	2	(Lee et al., 2021)
Commercial Activated Carbon (NORIT ® 830) (1)	**PFCA:** PFBA	1	(Inyang and Dickenson, 2017)
Biochars			
Biochars derived from maize straw and willow sawdust (2)	**PFSA:** PFOS	2	(Chen et al., 2011)
Biochars derived from different feedstocks (3)	**PFCA:** PFBA, PFOA	6	(Inyang and Dickenson, 2017)
Biochars derived from Spend Coffee Grounds and Mountain Crest Gardens (2)	**PFSA:** PFOS	2	(Steigerwald and Ray, 2021)
Commercial hardwood biochar (1)	**PFCA:** PFOA; **PFSA:** PFOS	2	(Zhi and Liu, 2018)
Bamboo-derived biochar (1)	**PFCA:** PFHxA, PFHpA, PFOA	3	(Du et al., 2015)

* additional characterization data from Ulrich et al. (2015); ** additional characterization data from Morlay et al. (2012); *** characterization data derived from this study.

Section S2. Evaluation of the predictive accuracy of the model

To evaluate the predictive accuracy of the model, the root square mean error (RMSE) and the residual predictive deviation (RPD) were calculated as:

$$\mathrm{RMSE} = \sqrt{\frac{\sum_{i=1}^{n} \left(m_i - p_i\right)^2}{N}}$$

where *m* are the measured values, *p* are the predicted values, *i* is the entry being tested and *N* is the total number of entries included in the model. The RPD was calculated as:

$$\mathrm{RPD} = \frac{\mathrm{SD}}{\mathrm{RMSE}}$$

where SD is the standard deviation of the original data. RPD values indicate the quality of the model: RPD values < 1.5 are considered poor; RPD values from 1.5 to 2.0 are acceptable; RPD values between 2.0 and 3.0 are good; and RPD values > 3.0 are excellent (Knight et al., 2019).

Figure S1. Particle size distribution of the sorbent materials

TB

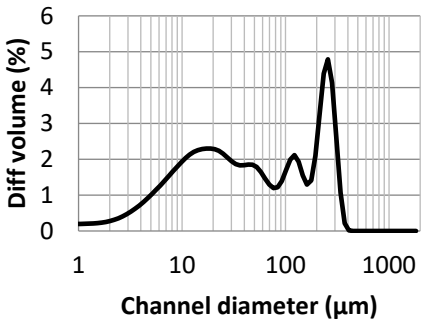

CE

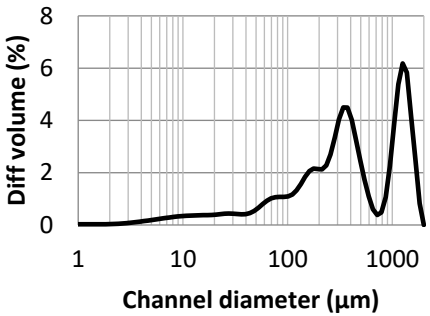

SB

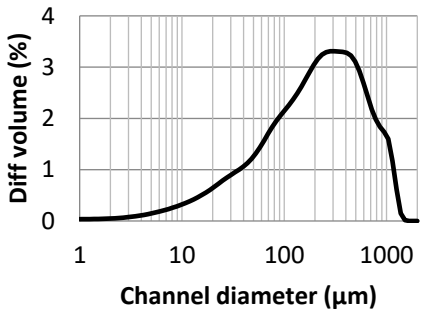

MOW

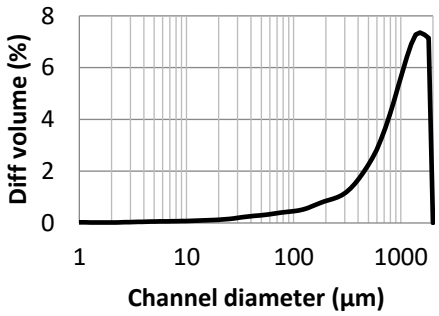

WH

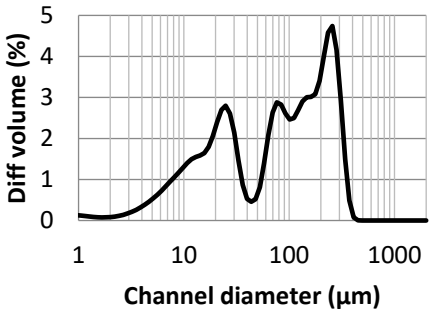

CM

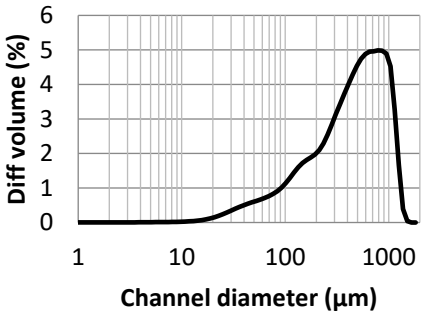

PC

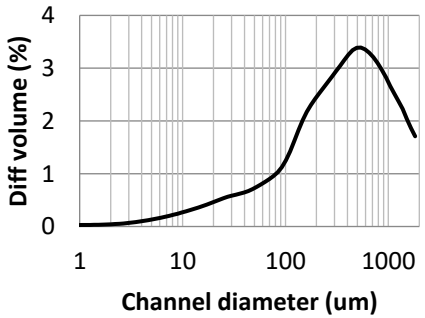

CF

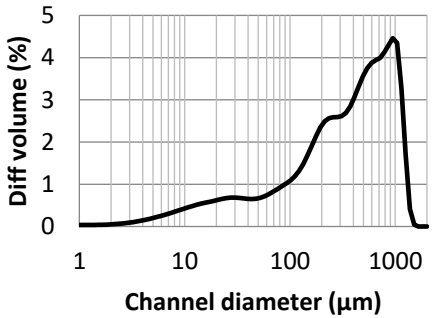

Figure S2. SEM images of the sorbent materials

TB

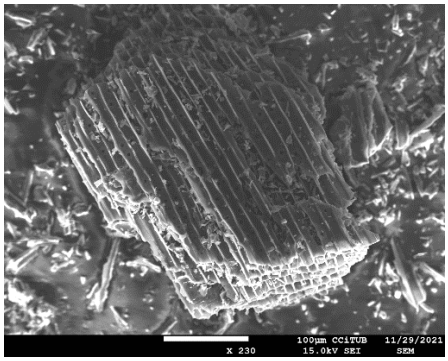

CE

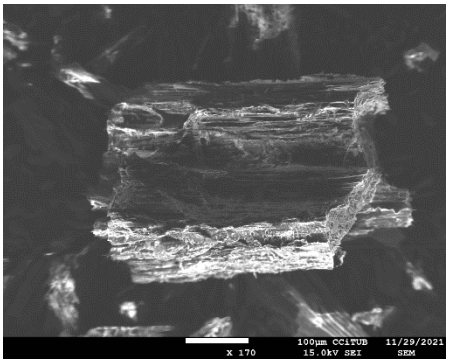

SB

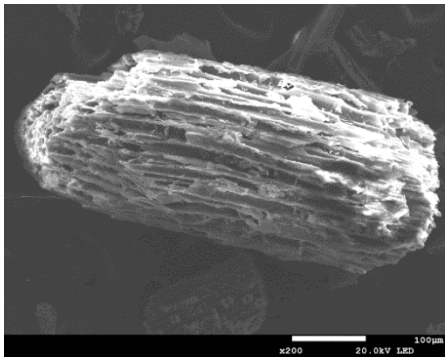

WH

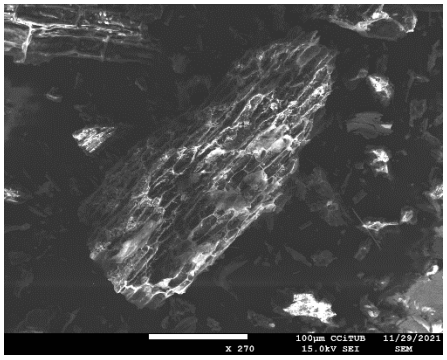

CM

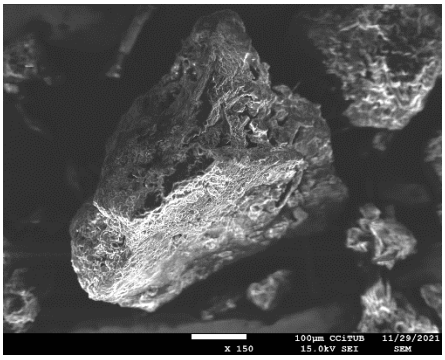

PC

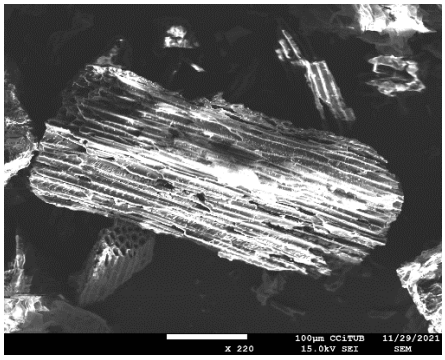

NGAC

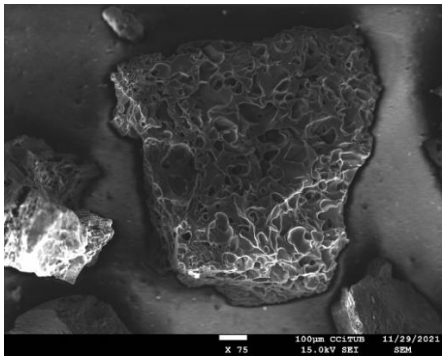

CF

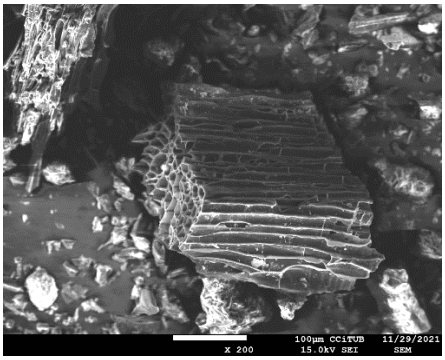

GAC

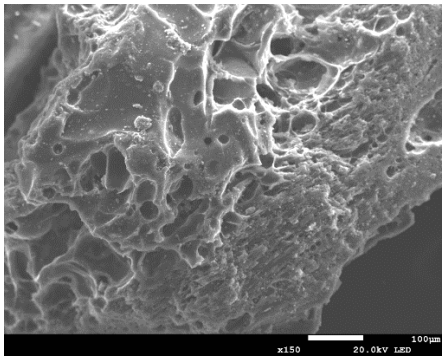

Table S4. Water soluble cations and anions of the sorbents

	TB	CE	SB	WH	CM	PC	MOW	CF	GAC	NGAC
Soluble cations										
Ca (meq L^{-1})	0.90	0.79	0.33	2.2	1.4	0.06	1.6	0.34	1.0	0.14
Mg (meq L^{-1})	0.22	1.8	0.38	25	2.0	0.35	1.8	0.31	1.6	0.02
K (meq L^{-1})	0.33	0.76	0.47	31	2.3	5.3	3.0	1.6	0.68	0.01
Na (meq L^{-1})	0.07	0.26	0.04	12	0.06	2.7	5.7	0.05	0.29	0.03
Soluble anions										
Cl (meq L^{-1})	0.20	1.4	0.07	58	0.85	12	8.8	0.31	0.33	0.05
SO_4 (meq L^{-1})	0.25	2.3	0.03	1.8	1.1	0.08	1.8	0.22	1.9	0.04
NO_3 (meq L^{-1})	0.41	0.17	n.d.	n.d.	n.d.	n.d.	0.25	1.7	0.02	0.01
PO_4 (meq L^{-1})	0.03	n.d.	n.d.	n.d.	1.6	1.6	0.19	n.d.	0.01	n.d.

n.d. not detected

Figure S3. FTIR spectra of the sorbent materials

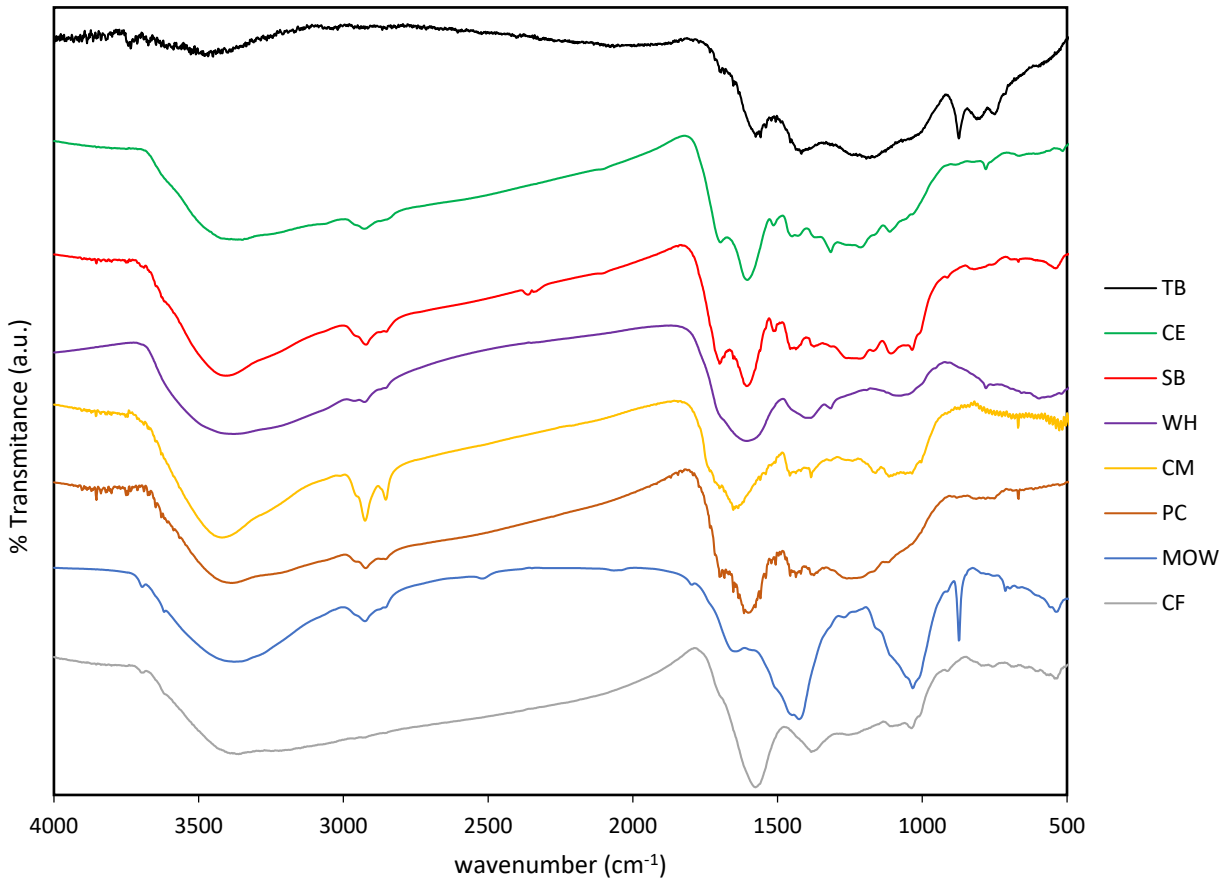

Table S5. PSOM kinetics results of PFOS sorption on materials TB, CE, MOW and CF.

Material	Experimental $C_{s,max}$ (ng g^{-1})	PSOM $C_{s,max}$ (ng g^{-1})	V_0 (ng g^{-1} h^{-1})	K_2 ($x10^{-3}$) (g ng^{-1} h^{-1})	r^2
TB	9.9×10^3	9.9×10^3	1.6×10^5	1.6	0.999
CE	7.4×10^3	7.4×10^3	1.1×10^5	2.0	0.999
MOW	8.2×10^3	8.4×10^3	7.7×10^3	0.11	0.998
CF	6.25×10^3	6.6×10^3	1.0×10^4	0.24	0.998

V_0 = initial PSOM rate constant; K_2 = PSOM rate constant

References

Carter, K. E., Farrell, J. 2010. Removal of perfluorooctane and perfluorobutane sulfonate from water via carbon adsorption and ion exchange. Sep. Sci. Technol. 45 (6), 762–767. https://doi.org/10.1080/01496391003608421

Chen, X., Xia, X., Wang, X., Qiao, J., Chen, H. 2011. A comparative study on sorption of perfluorooctane sulfonate (PFOS) by chars, ash and carbon nanotubes. Chemosphere, 83 (10), 1313–1319. https://doi.org/10.1016/j.chemosphere.2011.04.018

Deng, S., Zhang, Q., Nie, Y., Wei, H., Wang, B., Huang, J., Yu, G., Xing, B. 2012. Sorption mechanisms of perfluorinated compounds on carbon nanotubes. Environ. Pollut. 168, 138–144. https://doi.org/10.1016/j.envpol.2012.03.048

Du, Z., Deng, S., Chen, Y., Wang, B., Huang, J., Wang, Y., Yu, G. 2015. Removal of perfluorinated carboxylates from washing wastewater of perfluorooctanesulfonyl fluoride using activated carbons and resins. J. Hazard. Mater. 286, 136–143. https://doi.org/10.1016/j.jhazmat.2014.12.037

Inyang, M., Dickenson, E. R. V. 2017. The use of carbon adsorbents for the removal of perfluoroalkyl acids from potable reuse systems. Chemosphere, 184, 168–175. https://doi.org/10.1016/j.chemosphere.2017.05.161

Kelly, B. C., Ikonomou, M. G., Blair, J. D., Surridge, B., Hoover, D., Grace, R., Gobas, A. P. C. F. 2009. Perfluoroalkyl Contaminants in an Arctic Marine Food Web: Trophic Magnification and Wildlife Exposure. Env. Sci. Thecnol. 43, 4037–4043.

Knight, E. R., Janik, L. J., Navarro, D. A., Kookana, R. S., McLaughlin, M. J. 2019. Predicting partitioning of radiolabelled 14C-PFOA in a range of soils using diffuse reflectance infrared spectroscopy. Sci. Total Environ. 686, 505–513. https://doi.org/10.1016/j.scitotenv.2019.05.339

Lee, D. Y., Choi, G. H., Megson, D., Oh, K. Y., Choi, I. W., Seo, D. C., Kim, J. H. 2021. Effect of soil organic matter on the plant uptake of perfluorooctanoic acid (PFOA) and perfluorooctanesulphonic acid (PFOS) in lettuce on granular activated carbon-applied soil. Environ. Geochem. Hlth. 43, 2193 - 2202. https://doi.org/10.1007/s10653-020-00793-y

Meng, P., Fang, X., Maimaiti, A., Yu, G., Deng, S. 2019. Efficient removal of perfluorinated compounds from water using a regenerable magnetic activated carbon. Chemosphere, 224, 187–194. https://doi.org/10.1016/j.chemosphere.2019.02.132

Morlay, C., Quivet, E., Pilshofer, M., Faure, R., Joly, J. P. 2012. Adsorption of Imazamox herbicide onto Filtrasorb 400 activated carbon. J. Porous Mat. 19 (1), 79–86. https://doi.org/10.1007/s10934-011-9450-4

Ochoa-Herrera, V., Sierra-Alvarez, R. 2008. Removal of perfluorinated surfactants by sorption onto granular activated carbon, zeolite and sludge. Chemosphere, 72 (10), 1588–1593. https://doi.org/10.1016/j.chemosphere.2008.04.029

Senevirathna, S. T. M. L. D., Tanaka, S., Fujii, S., Kunacheva, C., Harada, H., Ariyadasa, B. H. A. K. T., Shivakoti, B. R. 2010. Adsorption of perfluorooctane sulfonate (n-PFOS) onto non ion-exchange polymers and granular activated carbon: Batch and column test. Desalination, 260, 29–33. https://doi.org/10.1016/j.desal.2010.05.005

Stebel, E. K., Pike, K. A., Nguyen, H., Hartmann, H. A., Klonowski, M. J., Lawrence, M. G., Collins, R. M., Hefner, C. E., Edmiston, P. L. 2019. Absorption of short-chain to long-chain perfluoroalkyl substances using swellable organically modified silica. Environ. Sci-Wat. Res. 5 (11), 1854–1866. https://doi.org/10.1039/c9ew00364a

Steigerwald, J. M., Ray, J. R. 2021. Adsorption behavior of perfluorooctanesulfonate (PFOS) onto activated spent coffee grounds biochar in synthetic wastewater effluent. J. Hazard. Mater. Letters. 2, 100025. https://doi.org/10.1016/j.hazl.2021.100025

Ulrich, B. A., Im, E. A., Werner, D., Higgins, C. P. 2015. Biochar and activated carbon for enhanced trace organic contaminant retention in stormwater infiltration systems. Environ. Sci. Technol. 49 (10), 6222–6230. https://doi.org/10.1021/acs.est.5b00376

Yan, B., Munoz, G., Sauvé, S., Liu, J. 2020. Molecular mechanisms of per- and polyfluoroalkyl substances on a modified clay: a combined experimental and molecular simulation study. Water Res. 184, 116166. https://doi.org/10.1016/j.watres.2020.116166

Yao, Y., Volchek, K., Brown, C. E., Robinson, A., Obal, T. 2014. Comparative study on adsorption of perfluorooctane sulfonate (PFOS) and perfluorooctanoate (PFOA) by different adsorbents in water. Water Sci. Technol. 70 (12), 1983–1991. https://doi.org/10.2166/wst.2014.445

Yu, Q., Zhang, R., Deng, S., Huang, J., Yu, G. 2009. Sorption of perfluorooctane sulfonate and perfluorooctanoate on activated carbons and resin: Kinetic and isotherm study. Water Res. 43 (4), 1150–1158. https://doi.org/10.1016/j.watres.2008.12.001

Zhi, Y., Liu, J. 2018. Sorption and desorption of anionic, cationic and zwitterionic polyfluoroalkyl substances by soil organic matter and pyrogenic carbonaceous materials. Chem. Eng. J. 346, 682–691. https://doi.org/10.1016/j.cej.2018.04.042